Data fusion-based structural damage detection under varying temperature conditions

Yuequan Bao[1, 2], Yong Xia[1*], Hui Li[2], You-lin Xu[1], and Peng Zhang[1]

[1]*Department of Civil and Structural Engineering, The Hong Kong Polytechnic University, Hong Kong, China*

[2]*School of Civil Engineering, Harbin Institute of Technology, Harbin, 150090, China*

* Corresponding author

Tel.: 852-2766 6066

E-mail: ceyxia@polyu.edu.hk

Abstract: A huge number of data can be obtained continuously from a number of sensors in long-term structural health monitoring (SHM). Different sets of data measured at different times may lead to inconsistent monitoring results. In addition, structural responses vary with the changing environmental conditions, particularly temperature. The variation in structural responses caused by temperature changes may mask the variation caused by structural damages. Integration and interpretation of various types of data are critical to the effective use of SHM systems for structural condition assessment and damage detection. A data fusion-based damage detection approach under varying temperature conditions is presented. The Bayesian-based damage detection technique, in which both temperature and structural parameters are the variables of the modal properties (frequencies and mode shapes), is developed. Accordingly, the probability density functions of the modal data are derived for damage detection. The damage detection results from each set of modal data and temperature data may be inconsistent because of uncertainties. The Dempster-Shafer (D-S) evidence theory is then employed to integrate the individual damage detection results from the different data sets at different times to obtain a consistent decision. An experiment on a two-story portal frame is conducted to demonstrate the effectiveness of the proposed method, with consideration on model uncertainty, measurement noise, and temperature effect. The damage detection results obtained by combining the damage basic probability assignments from each set of test data are more accurate than those obtained from each test data separately. Eliminating the temperature effect on the vibration properties can improve the damage detection accuracy. In particular, the proposed technique can detect even the slightest damage that is not detected by common damage detection methods in which the temperature effect is not eliminated.

Keywords: structural damage detection; temperature effect; data fusion; Dempster-Shafer evidence theory

1 Introduction

For the past 20 years, a number of damage identification methods have been developed and applied in aerospace, mechanical, and civil communities [1]. Most of these methods utilize the changes in structural vibration data and are usually based on either measured signals directly or numerical models. However, the inevitable measurement noise and the inaccurate finite element model [2, 3] limit the successful application of these methods to large-scale civil structures [4, 5].

The information fusion technique is a powerful tool for dealing with uncertainties. This technique has been widely applied in structural damage detection because of its inherent capability of extracting information from different sources and combining them into consistent, accurate, and intelligible information. The Bayesian theory and the Dempster-Shafer (D-S) evidence theory [6–13] are information fusion techniques popularly used for structural damage detection. The basic strategy of the Bayesian methods is that the posteriori probabilities can be updated based on the prior probabilities and conditional probabilities of the measured data using the Bayesian inference formula. As an extension of the Bayesian theory, the D-S evidence theory has been developed to combine multi-information following certain combination rules to reduce the uncertainties. Some researchers have investigated the application of the D-S evidence theory to structural damage detection [11–13].

Recently, studies have noted that environmental factors, such as temperature, humidity, water table, and freeze and thaw conditions, alter structural responses and, consequently, the structural vibration properties [14]. In addition, the variations in the vibration properties can be larger than those caused by structural damages. As a result, neglect of the environmental effects may lead to false damage detection.

Wipf [15] studied the relationship between long-term movements of a bridge and ambient temperature. In the study of the Alamosa Canyon Bridge, Sohn et al. [16] presented a linear adaptive model to discriminate between the change in modal parameters due to temperature changes and those due to structural damage or other environmental factors. Peeters and De

Roeck [17] developed a black-box ARX model to describe the variation in frequencies of the Z24-Bridge in Switzerland as a function of temperature. Ko et al. [18] used neural networks to investigate the relation between the natural frequencies and temperature of the Ting Kau cable-stayed bridge based on one-year field measurement data. Xia et al. [19] investigated the variation in frequencies, mode shapes, and damping, with respect to temperature and humidity changes in an experimental reinforced concrete slab. Linear models between the modal parameters and temperature and humidity have been established. Xia et al. [20] further investigated the non-uniform temperature effects on structural frequencies. Based on a sensitivity model-based technique, Kess [21] used a variability test matrix to isolate operational and environmental variability for a woven composite plate and to minimize the variability of damage indicators. Based on a subspace residue and χ^2-type global and sensitivity tests, Balmes [22] applied an extended detection algorithm to a simulated bridge deck. Xu and Wu [23] investigated the changes in frequencies and mode shape curvatures caused by average (seasonal) and asymmetric (sunshine) temperature variations in a cable-stayed bridge. Their results show that the frequency changes caused by temperature variation mask the frequency changes caused by damages. Yan et al. [24] proposed a principal components analysis-based damage detection method, with consideration on environmental conditions.

Clearly, measurement noise, modeling errors, and varying environmental conditions are inevitable in practical civil structures. Therefore, these factors should be considered appropriately in damage detection and other structural health monitoring applications. Bao et al. [25] proposed a D-S evidence theory-based damage identification method through the Bayesian approach, in which the measurement noise from multiple sets of data and the modeling errors are included. However, the variation in temperatures has not been considered. The current paper extends the previous study and presents a data fusion-based damage detection method under varying temperature conditions. The relation between the modal properties and the structural temperature is investigated and is subsequently used to eliminate the temperature effect on the vibration properties. All the vibration data measured under different conditions are transferred to those under the same reference temperature. Subsequently, the previously developed D-S data

fusion theory is employed for damage detection or condition assessment. Application of the developed data fusion method to a laboratory-based experiment shows that this method can detect the slightest artificial damage in a portal frame, which cannot be detected without considering temperature changes.

2 D-S Evidence Theory-based Data Fusion

2.1 Basic principle of data fusion

Data fusion was first proposed in the 1970s [26] and was developed in the 1980s alongside the rapid development of sensor techniques and computer technologies. Data fusion is a technique that uses computers to analyze automatically, integrate, and utilize spatial-temporal multi-sensor information through certain rules. Consequently, data fusion can explain and describe the measured objects consistently as well as fulfill the decision-making and evaluation tasks competently [26].

According to the data abstraction hierarchy, data fusion can be categorized into three levels: pixel level, eigen level, and decision level [26]. At the pixel level, the original data collected are summarized and analyzed before processing. At the eigen level, the important features from the original information, as measured from multiple sensors, are extracted. The decision level, also the top level, is where the final results for decision-making are obtained. Methods for decision fusion include the Bayesian fusion, the D-S evidence theory, and the fuzzy fusion. Differences between the D-S theory and the Bayesian theory have been presented by Klein [27]. In the present paper, the D-S evidence theory is employed as the data fusion technique for damage detection. A brief introduction to the D-S theory is given as follows.

The D-S evidence theory uses the basic probability assignment function (BPA), the belief function (Bel), and the plausibility function (Pl) to quantify evidence and its uncertainty [28]. For a finite set of mutually exclusive and exhaustive propositions Ω, also known as a frame of discernment, a power set 2^{Ω} is the set of all the subsets of Ω, including itself and a null set ϕ. The BPA, represented by *m*, is a function defined as $m: 2^{\Omega} \rightarrow [0, 1]$, such that

$$m(\phi)=0 \tag{1}$$

$$\sum_{A\in 2^{\Omega}} m(A)=1 \tag{2}$$

Respectively, the *Bel* and *Pl* measures are

$$Bel(A)=\sum_{B|B\subseteq A} m(B) \quad \text{and} \tag{3}$$

$$Pl(A)=\sum_{B|B\cap A\neq\varphi} m(B), \tag{4}$$

where *A* and *B* are the subsets of the power set, *Bel* represents the minimal confidence that a proposition lies in *A* or any subsets of *A*, and *Pl* represents the maximal confidence that one believes *A*. These two measures are the lower and upper bounds of belief of *A,* respectively.

The measures of evidence (i.e., BPA) from different resources can be combined using Dempster's rule of combination. As an example, two information sources, S_1 and S_2, are considered; $m_1(B)$ and $m_2(C)$ are the basic probability assignments given by sources S_1 and S_2, respectively. The combination rule is

$$m(A)=(1-k)^{-1}\sum_{B\cap C=A} m_1(B)m_2(C) \tag{5}$$

$$k=\sum_{B\cap C=\varphi} m_1(B)m_2(C), \tag{6}$$

where *k* is the basic probability mass associated with the conflict between S_1 and S_2. Item (1-*k*) compensates for the loss of non-zero probability assignments to non-intersecting subsets and ensures that the summation of probability assignments of the resultant BPA equals the unit. The Dempster's rule of combination is used to perform data fusion on the proposed damage detection method. Other combination rules can be found in Refs. 29–31.

An example is given to understand better Dempster's combination rule. Suppose two targets in a frame of discernment $\Omega=\{a_1,\ a_2\}$, then the power set is $2^{\Omega}=\{\phi,\ \{a_1\},\ \{a_2\},\Omega\}$. Considering two evidence sources S_1 and S_2, the BPAs from S_1 and S_2 assigned to $2^{\Omega}=\{\phi,\ \{a_1\},\ \{a_2\},\ \Omega\}$ are m_1 and m_2, respectively. Suppose the values of the BPAs are $m_1(\phi)=0$, $m_1(a_1)=0.6$, $m_1(a_2)=0.2$, $m_1(\Omega)=0.2$, $m_2(\phi)=0$, $m_2(a_1)=0.4$, $m_2(a_2)=0.5$, and $m_2(\Omega)=0.1$.

Table 1 illustrates the calculation.

Table 1. Example of Dempster's combination rule

m_2 \ m_1	$m_1(\phi)=0$	$m_1(a_1)=0.6$	$m_1(a_2)=0.2$	$m_1(\Omega)=0.2$
$m_2(\phi)=0$	$m(\phi)=0$	$m(\phi)=0$	$m(\phi)=0$	$m(\phi)=0$
$m_2(a_1)=0.4$	$m(\phi)=0$	$m(a_1)=0.24$	$m(\phi)=0.08$	$m(a_1)=0.08$
$m_2(a_2)=0.5$	$m(\phi)=0$	$m(\phi)=0.3$	$m(a_2)=0.1$	$m(a_2)=0.1$
$m_2(\Omega)=0.1$	$m(\phi)=0$	$m(a_1)=0.06$	$m(a_2)=0.02$	$m(\Omega)=0.02$

k is calculated as

$$k=\sum_{B\cap C=\phi} m_1(B)m_2(C)=0+0+0+0+0+0+0+0.3+0.08=0.38, \tag{7}$$

where B and C represent all the subsets of the power set 2^{Ω}.

The combined BPAs, m_{12}, is computed as

$$m_{12}(\phi)=0 \tag{8}$$

$$m_{12}(a_1)=(1-k)^{-1}\sum_{B\cap C=\{H_d\}} m_1(B)m_2(C)=\frac{0.24+0.06+0.08}{1-0.38}=0.6129 \tag{9}$$

$$m_{12}(a_2)=(1-k)^{-1}\sum_{B\cap C=\{H_{ud}\}} m_1(B)m_2(C)=\frac{0.1+0.1+0.02}{1-0.38}=0.3548 \tag{10}$$

$$m_{12}(\Omega)=\frac{0.02}{1-0.38}=0.0323 \tag{11}$$

If the number of information sources is more than two, the evidence can also be combined one by one, as shown in Eqs. (5) and (6). Klein [27] and Shafer [28] provided a detailed description of the D-S evidence theory.

2.2 Application to damage detection

A system stiffness matrix $\mathbf{K}$ can be expressed as an assembly of N_θ element stiffness matrices as

$$\mathbf{K} = \sum_{i=1}^{N_\theta} \theta_i \mathbf{K}_i \,, \tag{12}$$

where $\mathbf{K}_i$ is the stiffness matrix of the *i*th element, θ_i $(0 \le \theta_i \le 1)$ is its stiffness parameter indicating the elemental damage index, and N_θ is the number of structural elements. The damage index of a unit indicates no damage; a value of zero implies complete damage of the element. An element is defined as damaged when θ_i value is less than a specified threshold. $\mathbf{K}_i$ can also be the stiffness matrix of a substructure.

Let $H_{i,d}$ and $H_{i,ud}$ denote the damaged and undamaged states of the *i*th element, respectively. According to the D-S evidence theory, the frame of discernment is defined as

$$\Omega_i = \left\{ H_{i,d},\, H_{i,ud} \right\}, \tag{13}$$

which is composed of two exhaustive and exclusive hypotheses. The power set 2^{Ω_i} is composed of four propositions:

$$2^{\Omega_i} = \left\{ \phi_i,\ \left\{ H_{i,d} \right\},\ \left\{ H_{i,ud} \right\},\ \Omega_i \right\}, \tag{14}$$

where the subset ϕ_i is an empty set, and Ω_i represents uncertainty or the unknown. The BPAs are defined for each structural element as the measures of the probability of the four propositions.

Sets of modal data are assumed to be estimated from long-term vibration data of the structure. The modal data in the *n*th test are referred to as $\hat{\mathbf{\Lambda}}_n$.

$$\hat{\mathbf{\Lambda}}_n = \left[\hat{\omega}_1^{(n)}, \ldots, \hat{\omega}_{N_m}^{(n)}, \hat{\boldsymbol{\varphi}}_1^{(n)T}, \ldots, \hat{\boldsymbol{\varphi}}_{N_m}^{(n)T} \right]^T, \tag{15}$$

where $\hat{\omega}_r^{(n)}$ and $\hat{\boldsymbol{\varphi}}_r^{(n)}$ denote the *r*th frequency and mode shape extracted from the *n*th data set, respectively. N_m is the number of the estimated modes, and superscript T denotes the

transpose of a matrix or vector. When the vibration test is repeated N_s times, the collection of N_s sets of modal data is denoted as $\hat{\mathbf{D}}_t = \left\{ \hat{\mathbf{\Lambda}}_1,\ \hat{\mathbf{\Lambda}}_2,\ \ldots,\ \hat{\mathbf{\Lambda}}_{N_s} \right\}$. N_s sets of data are used to calculate the distribution of the modal data of the group. The group data can be measured at one time or at different times under different temperature conditions. In long-term vibration tests, N_t groups of $\hat{\mathbf{D}}_t$ $\left(t = 1, 2, \ldots, N_t\right)$ are assumed to be available. Their BPAs are

$$m_0^{(i)}, m_1^{(i)}, m_2^{(i)}, \cdots, \text{and } m_{N_t}^{(i)},\ \ i = 1, 2, \cdots, N_\theta, \tag{16}$$

where $m_t^{(i)}$ $\left(t = 1,\ 2, \cdots, N_t\right)$ is the posterior BPAs of the four propositions of power set 2^{Ω_i} based on the *t*th group data $\hat{\mathbf{D}}_t$. The calculation of $m_t^{(i)}$ will be described in the next section. The BPAs of $m_0^{(i)}$ to $m_t^{(i)}$ are then combined recursively by the D-S combination rule, similar to that shown in Eqs. (5) and (6):

$$m_{012\cdots t}^{(i)}(\phi_i) = 0 \tag{17a}$$

$$m_{012\cdots t}^{(i)}(H_{i,d}) = \frac{1}{1\text{-}k_t^{(i)}}\left[m_{012\cdots(t-1)}^{(i)}(H_{i,d}) m_t^{(i)}(H_{i,d}) + m_{012\cdots(t-1)}^{(i)}(H_{i,d}) m_t^{(i)}(\Omega_i) + m_t^{(i)}(H_{i,d}) m_{012\cdots t-1}^{(i)}(\Omega_i) \right] \tag{17b}$$

$$m_{012\cdots t}^{(i)}(H_{i,ud}) = \frac{1}{1-k_t^{(i)}}\left[m_{012\cdots(t-1)}^{(i)}(H_{i,ud}) m_t^{(i)}(H_{i,ud}) + m_{012\cdots(t-1)}^{(i)}(H_{i,ud}) m_t^{(i)}(\Omega_i) + m_t^{(i)}(H_{i,ud}) m_{012\cdots(t-1)}^{(i)}(\Omega_i) \right] \tag{17c}$$

$$m_{012\cdots t}^{(i)}(\Omega_i) = \frac{1}{1-k_t^{(i)}} m_{012\cdots(t-1)}^{(i)}(\Theta_i) m_t^{(i)}(\Omega_i) \tag{17d}$$

$$k_t^{(i)} = m_{012\cdots(t-1)}^{(i)}\left(H_{i,d}\right) m_t^{(i)}\left(H_{i,ud}\right) + m_{012\cdots(t-1)}^{(i)}\left(H_{i,ud}\right) m_t^{(i)}\left(H_{i,d}\right), \tag{17e}$$

where $t = 1,\ 2,\ \cdots,\ N_t$, $i = 1,\ 2,\ \cdots,\ N_\theta$, and $m_{012\cdots t}^{(i)}$ is the BPA combining $m_0^{(i)}$ through $m_t^{(i)}$.

3 Bayesian-based Damage Detection Considering the Temperature Effect

In the Bayesian probabilistic damage detection methodology [32], the uncertainties in parameters

$\boldsymbol{\theta} = \left\{ \theta_1 \quad \theta_2 \quad \cdots \quad \theta_{N_\theta} \right\}^T$ are quantified in terms of probability density functions (PDFs) obtained from N_s sets of modal data $\hat{\mathbf{D}}_t$:

$$p\left(\hat{\mathbf{D}}_t \middle| \boldsymbol{\theta}\right) = \prod_{n=1}^{N_s} p\left(\hat{\boldsymbol{\Lambda}}_n \middle| \boldsymbol{\theta}\right) = \prod_{n=1}^{N_s} \prod_{r=1}^{N_m} p\left(\hat{\omega}_r^{(n)} \middle| \boldsymbol{\theta}\right) p\left(\hat{\boldsymbol{\varphi}}_r^{(n)} \middle| \boldsymbol{\theta}\right) \tag{18}$$

In this approach, the modal data are regarded only as a function of the structural parameters.

Considering the temperature effect on the modal data, the modal data are a function of both the structural parameters and temperature. Consequently, temperature is also a variable of the modal data. Thus, Eq. (18) is extended as

$$p\left(\hat{\mathbf{D}}_t \middle| \boldsymbol{\theta}, T\right) = \prod_{n=1}^{N_s} p\left(\hat{\boldsymbol{\Lambda}}_n \middle| \boldsymbol{\theta}, T\right) = \prod_{n=1}^{N_s} \prod_{r=1}^{N_m} p\left(\hat{\omega}_r^{(n)} \middle| \boldsymbol{\theta}, T\right) p\left(\hat{\boldsymbol{\varphi}}_r^{(n)} \middle| \boldsymbol{\theta}, T\right), \tag{19}$$

where T is the temperature. The observed frequency can be expressed as

$$\hat{\omega}_r\left(\boldsymbol{\theta}, T\right) = \omega_r\left(\boldsymbol{\theta}, T_0\right) + \Delta\hat{\omega}_r\left(\boldsymbol{\theta}, T\right) + e_{\hat{\omega}_r}, \tag{20}$$

where $\omega_r\left(\boldsymbol{\theta}, T_0\right)$ is the frequency at a reference temperature T_0, $\Delta\hat{\omega}_r\left(\boldsymbol{\theta}, T\right)$ is the variation in frequency caused by the temperature change, and $e_{\hat{\omega}_r}$ is the frequency error obeying a zero-mean Gaussian distribution with a variance ε_r^2, which is computed by

$$\varepsilon_r^2 = \frac{1}{N_s} \sum_{n=1}^{N_s} \left(\hat{\omega}_r^{(n)} - \overline{\omega}_r\right)^2, \tag{21}$$

where $\overline{\omega}_r$ is the mean of $\hat{\omega}_r^{(n)}$, $n = 1, 2, \ldots, N_s$. The PDF of the frequency is then calculated as

$$p\left(\hat{\omega}_r^2 \middle| \boldsymbol{\theta}, T\right) = c_1 \exp\left[-\frac{1}{2}\left(\frac{\hat{\omega}_r - \omega_r - \Delta\hat{\omega}_r}{\varepsilon_r}\right)^2\right], \tag{22}$$

where c_1 is a normalization constant.

Similarly, the measured mode shape including the temperature variable is

$$\hat{\boldsymbol{\varphi}}_r\left(\boldsymbol{\theta}, T\right) = \alpha_r \boldsymbol{\varphi}_r\left(\boldsymbol{\theta}, T_0\right) + \Delta\hat{\boldsymbol{\varphi}}_r\left(\boldsymbol{\theta}, T\right) + \mathbf{e}_{\hat{\boldsymbol{\varphi}}_r}, \tag{23}$$

where $\boldsymbol{\varphi}_r(\boldsymbol{\theta}, T_0)$ is the mode shape at the degrees of freedom measured at the reference temperature T_0, $\Delta\hat{\boldsymbol{\varphi}}_r(\boldsymbol{\theta}, T)$ is the variation caused by the temperature change, $\mathbf{e}_{\hat{\phi}_r}$ is the mode shape error, and α_r is a scaling factor. Consequently, the PDF of the mode shape is

$$p\left(\hat{\boldsymbol{\varphi}}_r^2 \middle| \boldsymbol{\theta}, T\right) = c_2 \exp\left[-\frac{1}{2} \frac{\boldsymbol{\varphi}_r^T \left(\mathbf{I} - \left(\hat{\boldsymbol{\varphi}}_r^{(n)} - \Delta\hat{\boldsymbol{\varphi}}_r^{(n)} \right) \left(\hat{\boldsymbol{\varphi}}_r^{(n)} - \Delta\hat{\boldsymbol{\varphi}}_r^{(n)} \right)^T \right) \boldsymbol{\varphi}_r}{\delta_r^2 \left\| \boldsymbol{\varphi}_r \right\|^2} \right] \tag{24}$$

$$\delta_r^2 = \frac{1}{N_s} \sum_{n=1}^{N_s} \frac{\left\| \hat{\boldsymbol{\varphi}}_r^{(n)} - \overline{\boldsymbol{\varphi}}_r \right\|^2}{\left\| \hat{\boldsymbol{\varphi}}_r^{(n)} \right\|^2} \tag{25}$$

$$\alpha_r = \frac{\left\langle \hat{\boldsymbol{\varphi}}_r, \boldsymbol{\varphi}_r \right\rangle}{\left\| \boldsymbol{\varphi}_r \right\|^2}, \tag{26}$$

where $\delta_r^2 \left\| \boldsymbol{\varphi}_r \right\|^2$ is the diagonal element of the covariance matrix of $\hat{\boldsymbol{\varphi}}_r$, and c_2 is a normalization constant. Eqs. (20) and (23) show a general relation between modal data and temperature. Given a specific relation, the PDFs of the modal data can be obtained explicitly or numerically. A case study in the next section demonstrates the procedures for eliminating the temperature effect from the frequencies and mode shapes.

The initial PDF of the model parameters $\boldsymbol{\theta}$ is assumed as

$$p\left(\boldsymbol{\theta} \middle| T\right) = c_3 \exp\left[-\frac{1}{2} \left(\boldsymbol{\theta} - \boldsymbol{\theta}_0 \right)^T \mathbf{S}^{-1} \left(\boldsymbol{\theta} - \boldsymbol{\theta}_0 \right) \right], \tag{27}$$

where **S** is a diagonal variance matrix of $\boldsymbol{\theta}$ and can be determined based on engineering experience or published references, c_3 is a normalization constant, and $\boldsymbol{\theta}_0$ is the initial value of $\boldsymbol{\theta}$ taking $\boldsymbol{\theta}_0 = \{1, 1, \ldots, 1\}^T$, indicating that no damage is present in the structure.

According to Eqs. (19), (22), (24), and (27), $p\left(\boldsymbol{\theta} \middle| \hat{\mathbf{D}}_t, T\right)$ is

$$p\left(\boldsymbol{\theta} \middle| \hat{\mathbf{D}}_t, T\right) = c p\left(\hat{\mathbf{D}}_t \middle| \boldsymbol{\theta}, T\right) p\left(\boldsymbol{\theta} \middle| T\right) = c \exp\left[-\frac{1}{2} J\left(\boldsymbol{\theta}\right) \right], \tag{28}$$

where

$$J(\boldsymbol{\theta}) = (\boldsymbol{\theta} - \boldsymbol{\theta}_0)^T \mathbf{S}^{-1} (\boldsymbol{\theta} - \boldsymbol{\theta}_0) + J_a, \tag{29}$$

$$J_a = \sum_{n=1}^{N_s} \sum_{r=1}^{N_m} \frac{\left(\hat{\omega}_r^{(n)} - \omega_r^{(n)} - \Delta\hat{\omega}_r^{(n)}\right)^2}{\varepsilon_r^{\,2}} + \frac{\boldsymbol{\varphi}_r^T \left(\mathbf{I} - \left(\hat{\boldsymbol{\varphi}}_r^{(n)} - \Delta\hat{\boldsymbol{\varphi}}_r^{(n)}\right)\left(\hat{\boldsymbol{\varphi}}_r^{(n)} - \Delta\hat{\boldsymbol{\varphi}}_r^{(n)}\right)^T\right)\boldsymbol{\varphi}_r}{\delta_r^2 \left\|\boldsymbol{\varphi}_r\right\|^2}, \tag{30}$$

and c is the normalization constant.

The marginal PDFs of θ_i can be obtained by integrating the joint PDF in Eq. (28) using Laplace's method for asymptotic expansion [33]:

$$p\left(\theta_i \middle| \hat{\mathbf{D}}_t, T\right) \approx \psi\left(\frac{\theta_i - \hat{\theta}_i}{\hat{\sigma}_i}\right), \tag{31}$$

where ψ is the standard Gaussian PDF, $\hat{\theta}_i$ is the most probable model obtained by minimizing $J(\boldsymbol{\theta})$ in Eq. (29), and $\hat{\sigma}_i^2$ is the ith diagonal element of the Hessian matrix of $J(\boldsymbol{\theta})$ evaluated at $\hat{\boldsymbol{\theta}}$.

The damage probability of the ith substructure $P^{(i)}$ is defined as [29]

$$P^{(i)}(d_i) = P\left(\hat{\theta}_i^{pd} < (1-d_i)\hat{\theta}_i^{ud} \middle| \hat{\mathbf{D}}^{ud}, \hat{\mathbf{D}}^{pd}, T^{ud}, T^{pd}\right), \tag{32}$$

where $d_i \in [0,1]$ is the damage threshold of the ith member, superscripts *ud* and *pd* denote the quantities corresponding to the undamaged structure and the possibly damaged structure, respectively, and $\hat{\mathbf{D}}^{ud}$ and $\hat{\mathbf{D}}^{pd}$ are the group of modal data obtained from the undamaged structure and the possibly damaged structure at temperatures T^{ud} and T^{pd}, respectively. Using the Gaussian approximations for the marginal distributions, $P^{(i)}$ is calculated by [29]

$$P^{(i)}(d_i) \approx \Phi\left(\frac{(1-d_i)\hat{\theta}_i^{ud} - \hat{\theta}_i^{pd}}{\sqrt{(1-d_i)^2\left(\hat{\sigma}_i^{ud}\right)^2 + \left(\hat{\sigma}_i^{pd}\right)^2}}\right), \tag{33}$$

where $\Phi(\cdot)$ is the standard Gaussian cumulative distribution function.

The *t*th BPAs $m_t^{(i)}(\phi_i)$, $m_t^{(i)}(H_{i,d})$, $m_t^{(i)}(H_{i,ud})$, and $m_t^{(i)}(\Omega_i)$ ($t=1,\ 2,\cdots,N_t$) are then defined as follows:

$$m_t^{(i)}(\phi_i)=0, \tag{34a}$$

$$m_t^{(i)}(H_{i,d})=\eta\times P_t^{(i)}(d_i), \tag{34b}$$

$$m_t^{(i)}(H_{i,ud})=\eta\left(1-P_t^{(i)}(d_i)\right), \tag{34c}$$

$$m_t^{(i)}(\Omega_i)=1-m_t^{(i)}(H_{i,d})-m_t^{(i)}(H_{i,ud})=1-\eta, \tag{34d}$$

where $\eta\in[0,1]$ is the weighting coefficient reflecting the reliability of the damage decision of the member using the Bayesian method.

At the initial stage, data are unavailable for the calculation of BPAs. Therefore, the initial BPAs are defined as follows:

$$m_0^{(i)}(\varphi_i)=0;\ \ m_0^{(i)}(H_{i,d})=0;\ \ m_0^{(i)}(H_{i,ud})=0;\ \ m_0^{(i)}(\Omega_i)=1, \tag{35}$$

where $m_0^{(i)}(\Omega_i)=1$ implies that the damage state of the *i*th member has the maximum uncertainty.

The flow chart of the proposed damage identification procedure is shown in Fig. 1. The first step is to obtain the modal data sets $\hat{\mathbf{D}}_t\ (t=1,2,\ldots,N_t)$. Second, the temperature effect on the data sets is eliminated according to the relation between the temperature and the modal data. Third, initial BPAs calculated by Eq. (35) are updated using the measured multi-data sets in a progressive time sequence following the D-S combination rule. In the progressive updating procedures, the effect of uncertainties on damage detection decision obtained from individual data sets will be reduced, and the accuracy of the final damage detection decision can be improved.

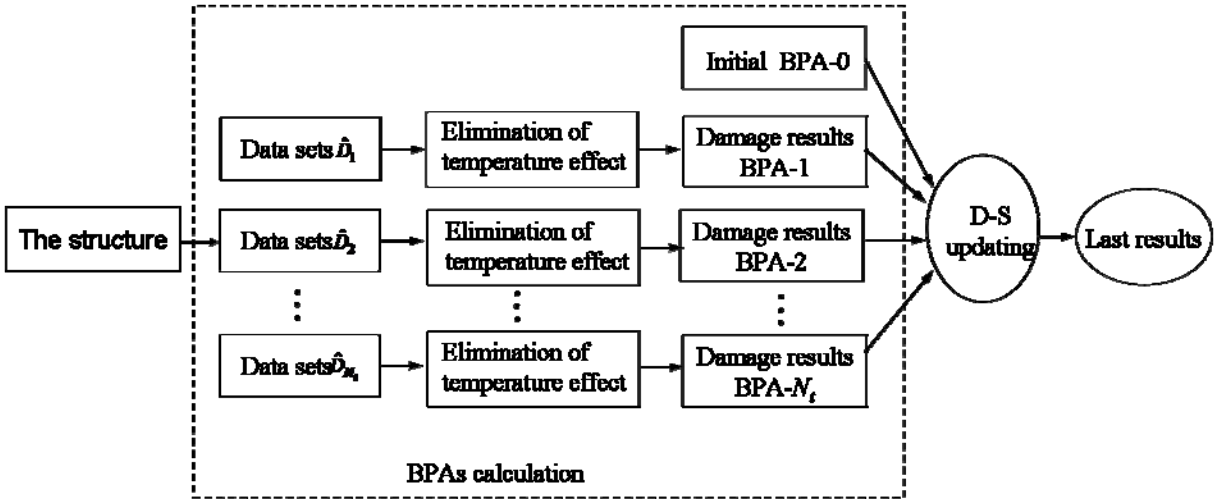

Fig. 1. Flow chart of the damage detection approach

4 Case Study

4.1 Introduction to the experiment

The experimental model is a two-storey steel frame structure, as shown in Fig. 2. The cross sections of the beam and column are 50.0×8.8 mm^2 and 50.0×4.4 mm^2, respectively. The mass density and Young's modulus are 7.67×10^3 kg/m^3 and 2.0×10^5 MPa, respectively. The detailed geometry and sensor locations of the frame are illustrated in Fig. 3. The frame is modelled using 20 planar Euler-Bernoulli beam elements.

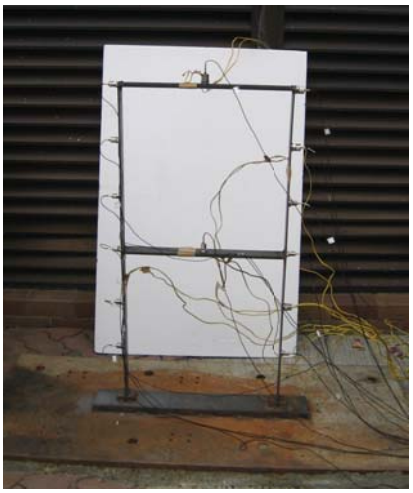

Fig. 2. Experimental model

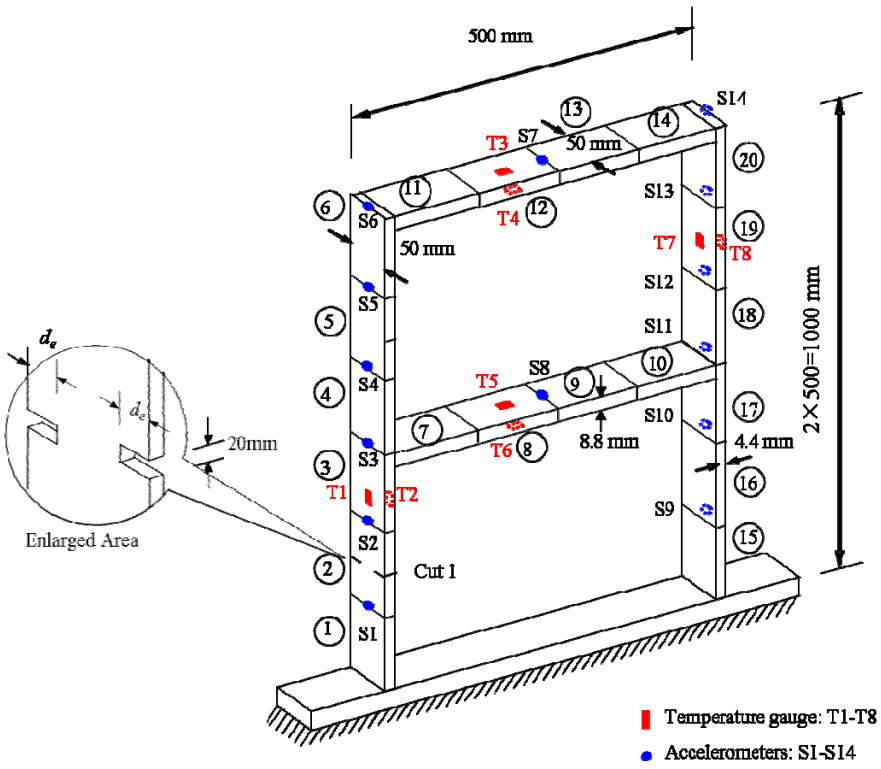

Fig. 3. Configuration of the frame

The frame was exposed to sunlight from morning to afternoon on August 27, 2010. The temperatures of the beams and columns were measured every 30 seconds using 8 thermocouples (T1–T8). The frame was excited using an instrumented hammer, and the vibration responses were recorded by 14 accelerometers (S1–S14). A total of 30,720 data points were collected at a sampling rate of 2,048 Hz for each hammer impact. The vibration tests were performed 5 times every 20 minutes. A total of $5 \times 28 = 140$ sets of vibration data were recorded throughout the day.

The damage was subsequently introduced by cutting the section of one column, as shown in Fig. 3. In this experiment, three damage scenarios are simulated by a cut length of 20 mm and depth d_e = 5, 10, and 15 mm, respectively. The equivalent losses of element bending stiffness for the three damage cases are about 3%, 7%, and 15%, respectively. In each damage scenario, a one-day vibration testing was conducted, and the temperature and vibration data were measured similarly, resulting in 140 sets of vibration data for each damage case.

The temperatures of the frame in the undamaged and one damaged states are shown in Fig. 4. The maximum variation in the structural temperature during the day occurred at about 30 °C. The peak temperature occurred at about 12:00. Clearly, the temperatures of the beams (T3–T6) are higher than those of columns (T1, T2, T7, and T8).

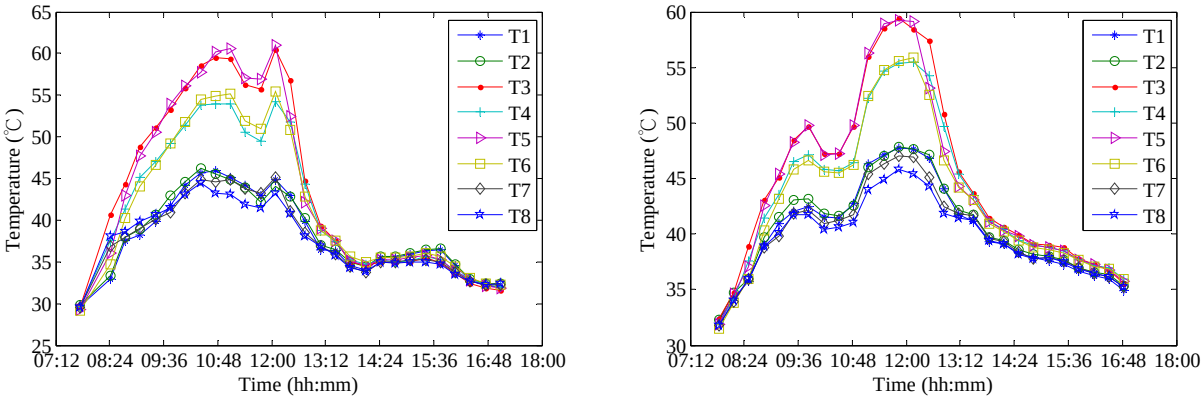

(a) Variation in temperature on August 27, 2010 (no damage)

(b) Variation in temperature on September 1, 2010 (d_e=10mm)

Fig. 4. Measured temperature of the frame

The first five mode shapes are shown in Fig. 5, in which the points and solid lines represent the experimental and analytical mode shapes, respectively, and the dashed lines are the undeformed model. The modal frequencies and mode shapes were identified using the rational fraction polynomial method [34].

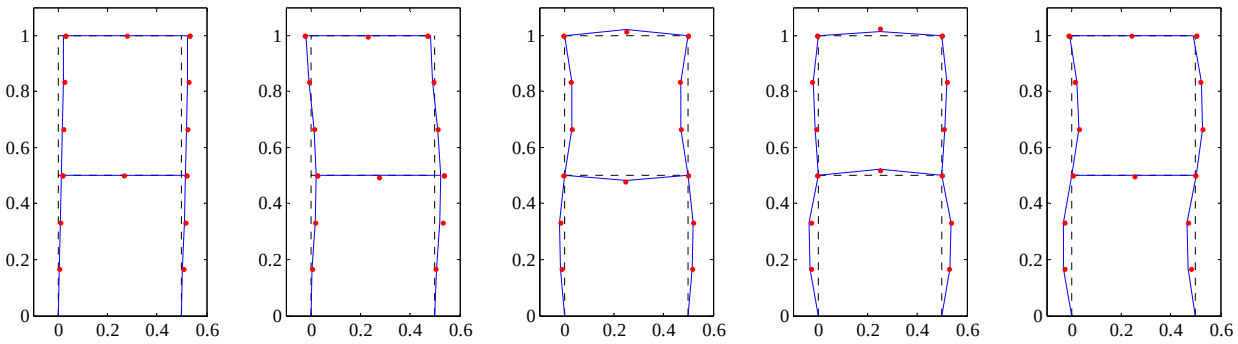

(a) Mode 1 (b) Mode 2 (c) Mode 3 (d) Mode 4 (e) Mode 5

Fig. 5. Analytical and experimental mode shapes of the undamaged structure

4.2 Relation of modal parameters with temperature

The relation between the first five modal frequencies and the temperature of the frame in all damage cases are shown in Fig. 6, in which the temperature is the mean value of the eight temperature gauges. The figure demonstrates that all five frequencies decrease with an increase in temperature. For most of the modes, the frequencies decrease with the increase in damage severity under the same temperature. In addition, the frequencies of the undamaged structure at a higher temperature are smaller than the frequencies of the slightly damaged structure (d_e = 5 mm) at a lower temperature, indicating that temperature has a more significant effect on the frequencies than do slight damage. In more severe damage cases of d_e = 10 and 15 mm, the changes in frequencies caused by the damage are larger than those caused by temperature change.

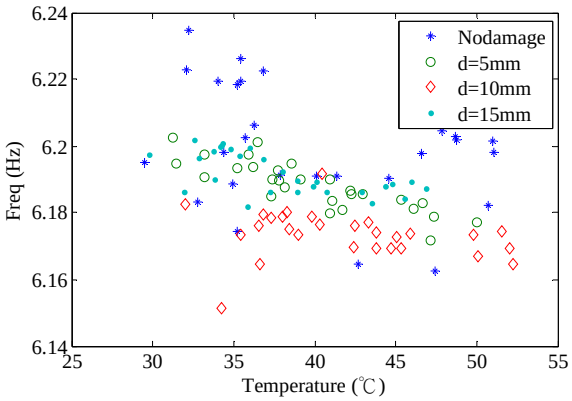

(a) First mode

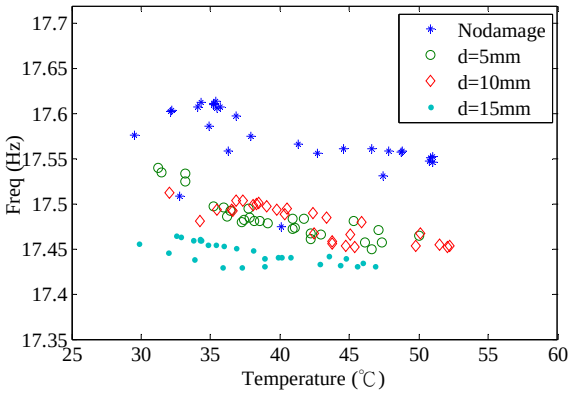

(b) Second mode

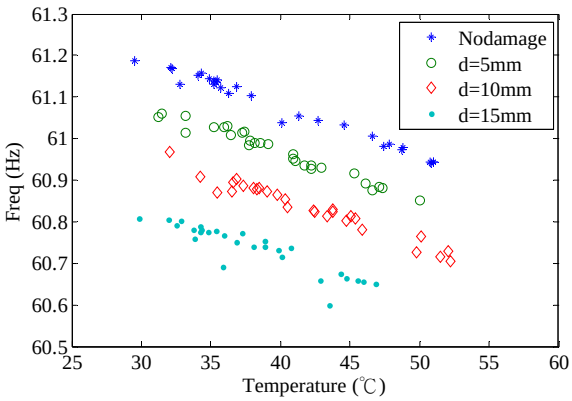

(c) Third mode

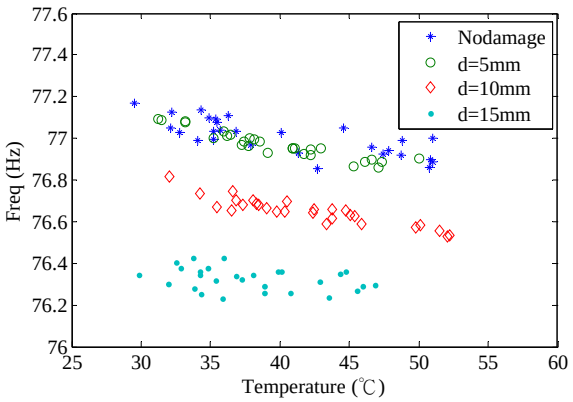

(d) Fourth mode

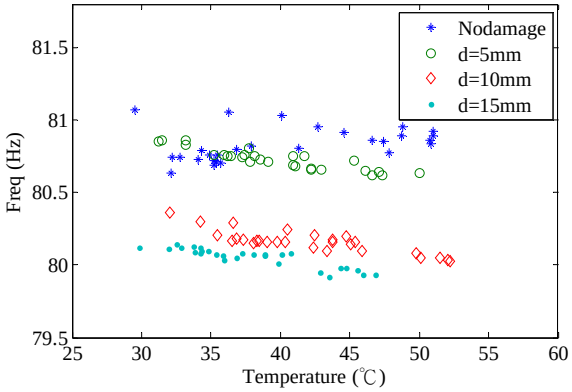

(e) Fifth mode

Fig. 6. Relation of the measured frequencies with temperature

To determine the effect of temperature on the mode shapes, the modal assurance criterion (MAC) [34] is investigated. The MAC value is defined as

$$MAC\left(\hat{\boldsymbol{\varphi}}_r, \boldsymbol{\varphi}_r\right) = \frac{\left|\hat{\boldsymbol{\varphi}}_r{}^T \boldsymbol{\varphi}_r\right|^2}{\left(\hat{\boldsymbol{\varphi}}_r{}^T \hat{\boldsymbol{\varphi}}_r\right)\left(\boldsymbol{\varphi}_r{}^T \boldsymbol{\varphi}_r\right)}, \tag{36}$$

where $\hat{\boldsymbol{\varphi}}_r$ and $\boldsymbol{\varphi}_r$ are the rth measured and theoretical mode shapes. If two mode shapes are identical, the MAC value will equal unity. Any variation in the mode shapes will generate a MAC value less than unity. The MAC values of the first five modes, with respect to the averaged temperature of the structure, are shown in Fig. 7. No clear relation between the MAC values and the temperature can be observed. The variations in the MAC values of the first five modes caused by the damage are significant, especially damage case d_e = 15mm.

Based on these observations, the variation in temperature has a significant effect on the structural vibration frequencies but not on mode shapes. Consequently, only the temperature effect on frequencies is eliminated in the damage detection in the current study.

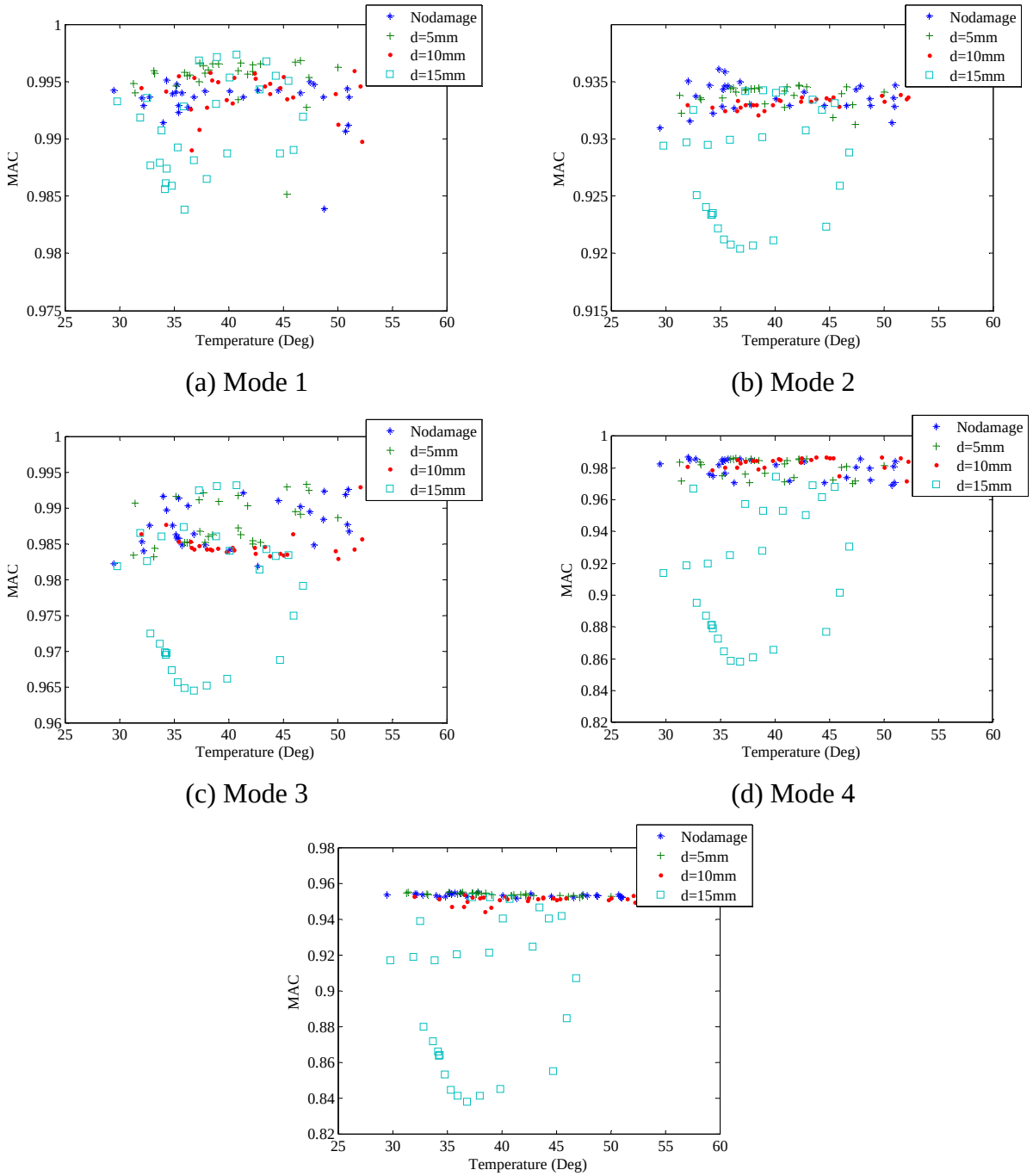

(a) Mode 1

(b) Mode 2

(c) Mode 3

(d) Mode 4

(e) Mode 5

Fig. 7. Relation of the measured mode shapes with temperature

4.3 Elimination of the temperature effect on frequencies

As the measured frequencies show a linear relation with temperature, a linear regression model between the frequency and temperature is established as

$$\hat{\omega}_r\left(\boldsymbol{\theta},T\right)=\beta_0^{(r)}+\beta_T^{(r)}T+\varepsilon_{\hat{\omega}_r}\,, \tag{37}$$

where $\beta_0^{(r)}$ (intercept) and $\beta_T^{(r)}$ (slope) are regression coefficients, and $\varepsilon_{\hat{\omega}_r}$ is the error of the *r*-th frequency. The regression coefficients can be obtained using least-squares fitting.

Next, a reference temperature T_0 is selected. The measured frequencies at temperature T can be transformed into those at the reference temperature by

$$\begin{aligned}\hat{\omega}_r^e\left(\boldsymbol{\theta},T\right)&=\hat{\omega}_r\left(\boldsymbol{\theta},T\right)-\Delta\hat{\omega}_r\left(\boldsymbol{\theta},\Delta T\right)\\&=\hat{\omega}_r\left(\boldsymbol{\theta},T\right)-\beta_T^{(r)}\left(T-T_0\right)\end{aligned}\,, \tag{38}$$

where $\hat{\omega}_r\left(\boldsymbol{\theta},T\right)$ is the measured frequency, and $\hat{\omega}_r^e\left(\boldsymbol{\theta},T\right)$ is the transformed frequency at temperature T_0. The third frequency of the undamaged frame is employed as an example, as shown in Fig. 8. The reference temperature is set to 40 °C. The measured frequency $\hat{\omega}_3\left(\boldsymbol{\theta},T_j\right)$ is transformed to $\hat{\omega}_3^e\left(\boldsymbol{\theta},T_0\right)$ by

$$\hat{\omega}_3^e\left(\boldsymbol{\theta},T_0\right)=\hat{\omega}_3\left(\boldsymbol{\theta},T_j\right)-\beta_T^{(3)}\left(T_j-T_0\right). \tag{39}$$

In this example, regression coefficients $\beta_0^{(3)}=61.5463\,\text{Hz}$, $\beta_T^{(3)}=-0.0118$ Hz/°C, and $\beta_T^{(3)}/\beta_0^{(3)}=-0.019\%$. This result indicates that a unit increase in temperature leads to a decrease in the frequency by 0.019%. In this manner, all frequencies measured under different temperature conditions can be transformed into those at the same temperature (40 °C), as shown in Fig. 9. The figure shows that the variation in frequencies caused by temperature has been removed.

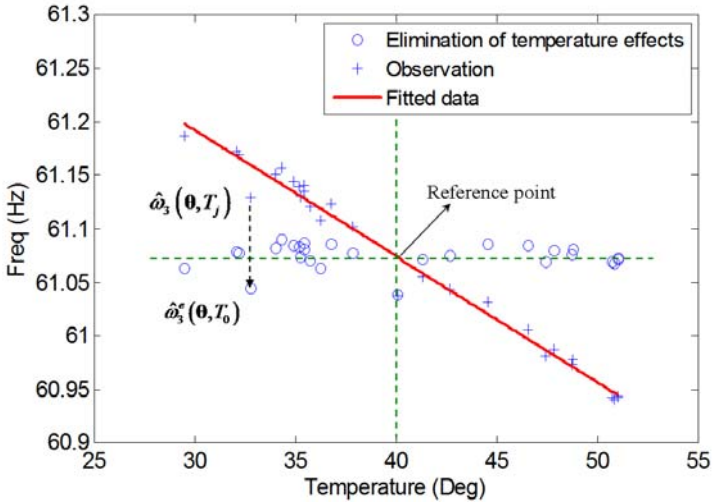

Fig. 8. Elimination of the temperature effect on the third frequency

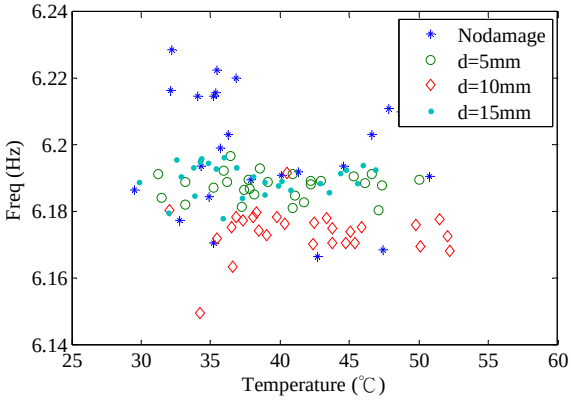

(a) First frequency

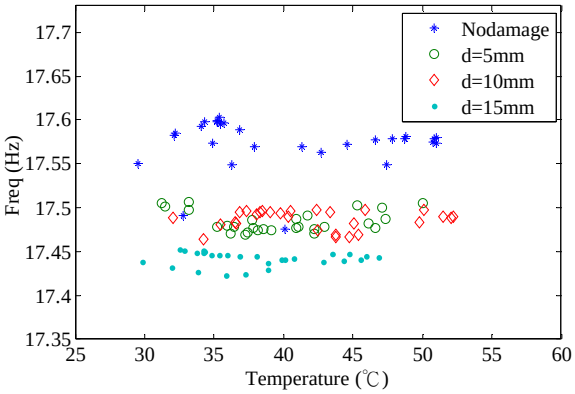

(b) Second frequency

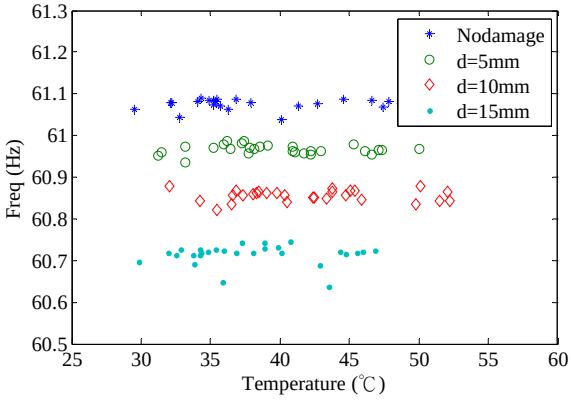

(c) Third frequency

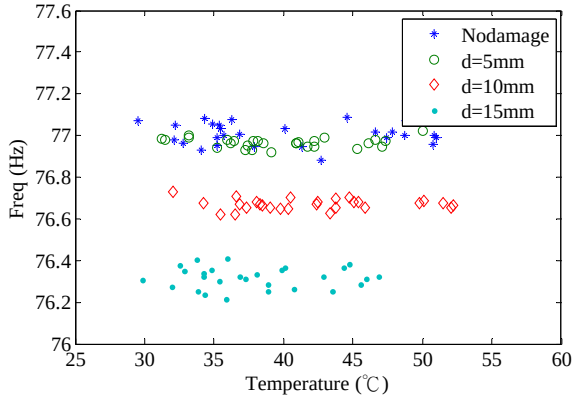

(d) Fourth frequency

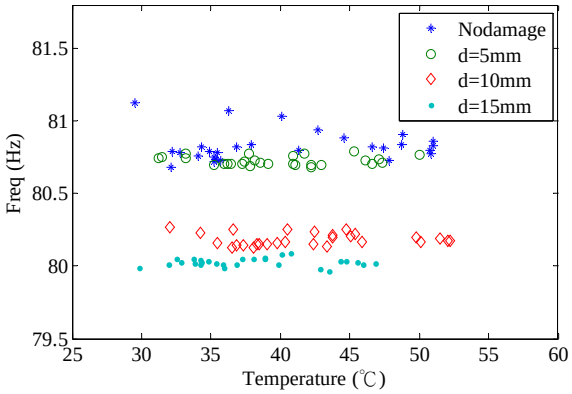

(e) Fifth frequency

Fig. 9. Elimination of temperature effect on the measured frequencies

4.4 Damage detection

As described in Section 4.1, a total of 140 sets of vibration data are measured in each damage case. Each set of data include the first five modal frequencies and mode shapes at the 14 sensor points. As the physical model has 20 elements, each having one unknown stiffness parameter. The optimisation problem is identifiable. The measured modal parameters are assorted into $N_t = 7$ groups, each with $N_s = 20$ sets of data $\hat{\mathbf{D}}_t = \left\{ \hat{\mathbf{\Lambda}}_1,\ \hat{\mathbf{\Lambda}}_2,\ \ldots,\ \hat{\mathbf{\Lambda}}_{N_s} \right\}$. As an example, PDFs of element 2 (θ_2) for the undamaged and damage case d_e = 10 mm are illustrated in Fig. 10. The mean value of θ_2 in the damaged state is smaller than that in the undamaged state. The BPAs of each element in each group ($m_0^{(i)}, m_1^{(i)}, m_2^{(i)}, \cdots, m_{N_t}^{(i)}$, $i = 1,\ 2,\ \cdots,\ N_\theta$, N_θ = 20 here) can be calculated using the method presented in Section 3. The weighting coefficient is estimated as $\eta = 0.85$ based on engineering experience. The BPAs from the seven groups of data are then combined using the D-S combination rule, as described previously.

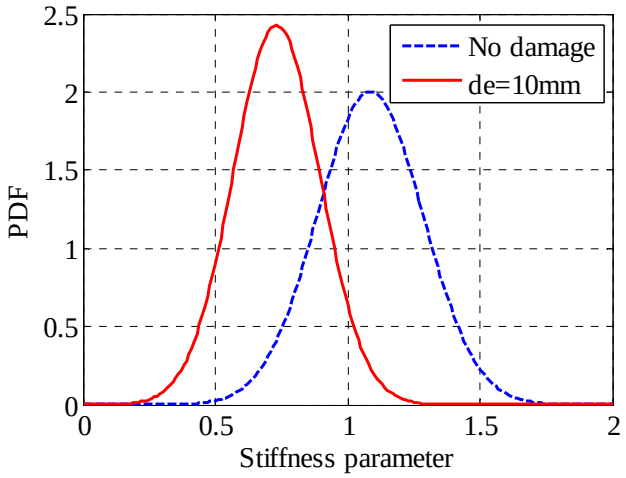

Fig. 10. One pair of PDFs of θ_2 for the undamaged and damage cases d_e = 10 mm without removing the temperature effect

Figs. 11–13 show the damage detection results using each group of data and the data fusion approach without eliminating the temperature effect for damage cases d_e = 5, 10, and 15 mm, respectively. The BPAs in the left column of the figures are those using the individual group of data; the right column shows the evolution of the BPAs when individual groups of data are combined. In particular, the BPAs of "Update 1" are the same as those of "Test 1" (the first group); the BPAs of "Update 2" combine the BPAs of "Test 1" and "Test 2" (the second group) using the D-S combination rule; and "Update 7" gives the final BPAs, integrating all seven groups of data. Fig. 11 indicates that this small damage cannot be identified even if all groups of data are combined. When the extent of the damage increases to d_e = 10 mm, the damage located at element 2 can be identified correctly using the D-S combination rule, as shown in Fig. 12. However, element 7 is incorrectly identified as damaged. Fig. 13 shows the damage detection results of damage case d_e = 15 mm, in which the true damage can be detected correctly. Figs. 12 and 13 illustrate that the damage detection results obtained by combining the damaged BPAs from the seven groups of data through the D-S method are better than the results obtained using each group of data exclusively; if more groups are combined, better damage identification results are achieved.

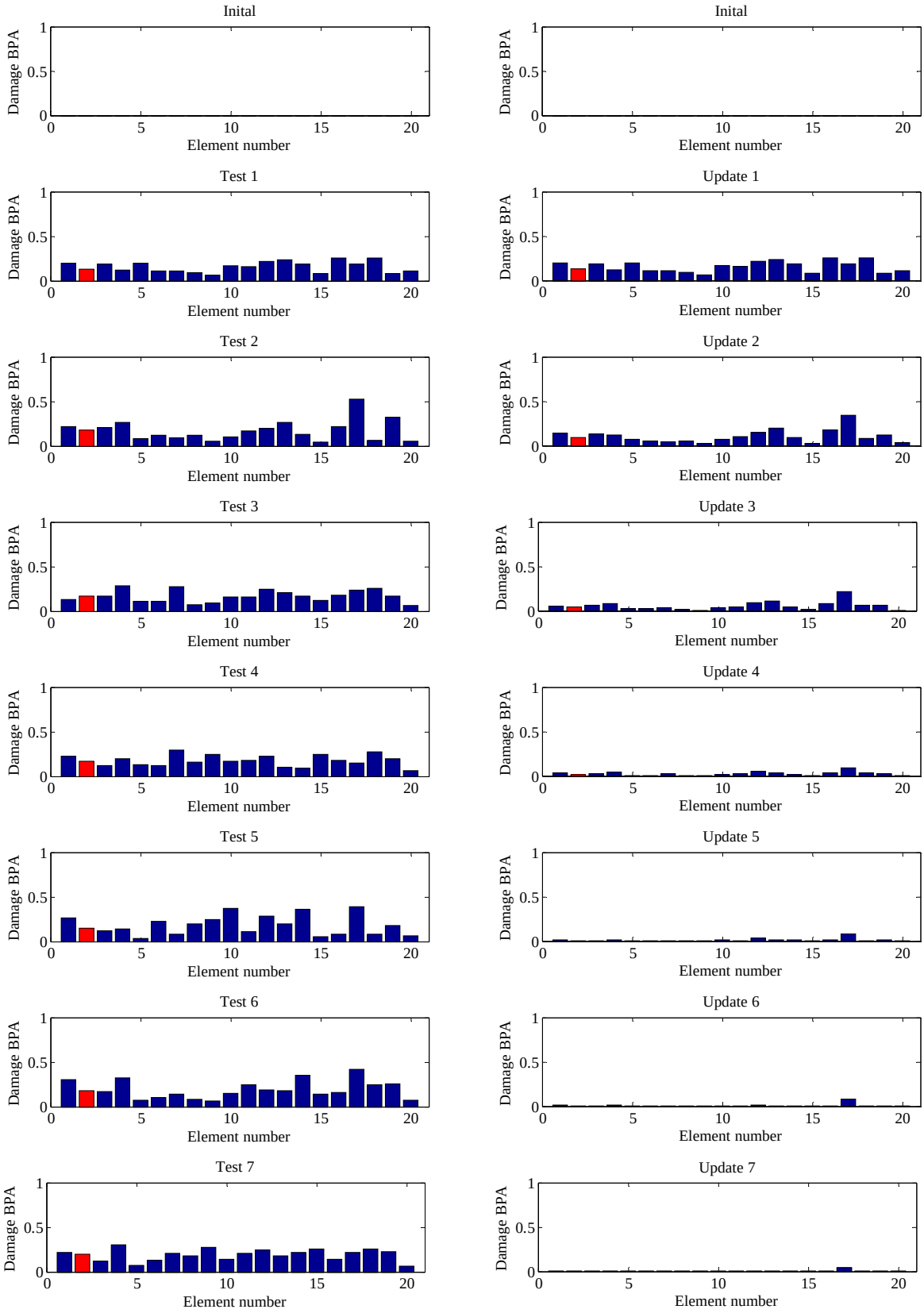

(a) Each test result (b) D-S fusion results

Fig. 11. Damage detection results of damage case d_e = 5 mm without considering the temperature effect

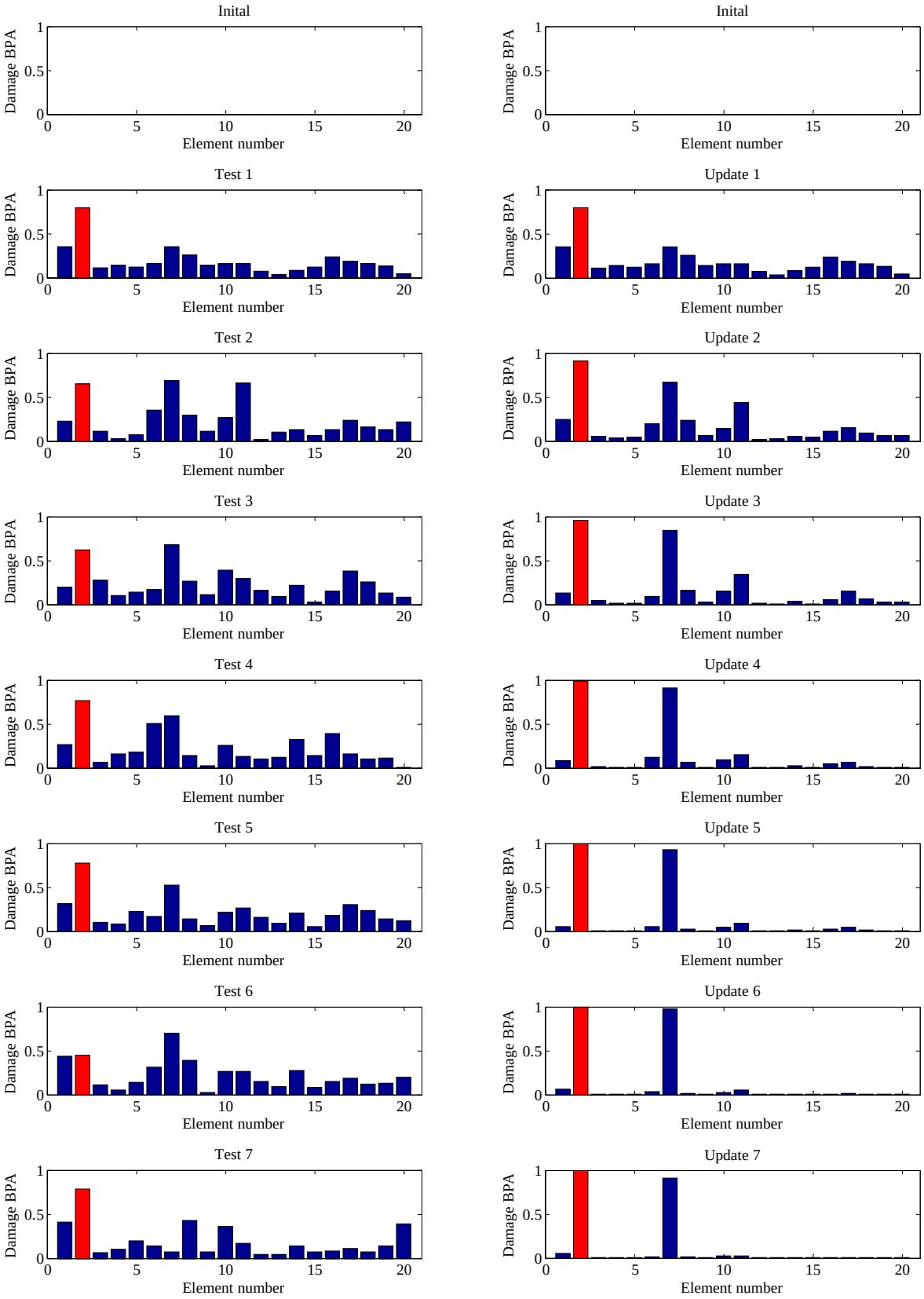

(a) Each test result (b) D-S fusion results

Fig. 12. Damage detection results of damage case d_e= 10 mm without considering the temperature effect

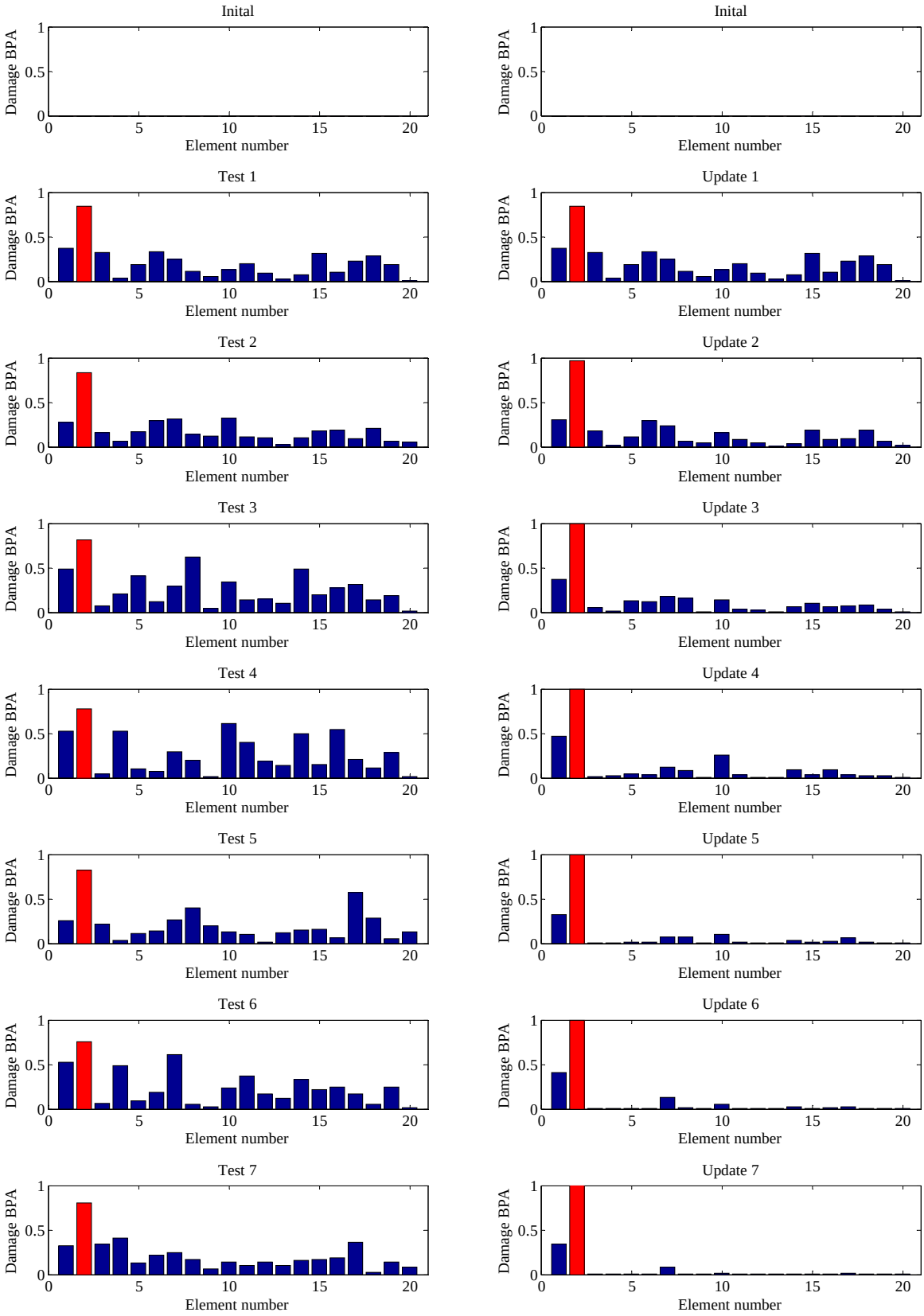

(a) Each test result (b) D-S fusion results

Fig. 13. Damage detection results of damage case d_e = 15 mm without considering the temperature effect

These results verify that the slightest damage cannot be identified correctly without considering the variation in temperatures, although the uncertainties in the measurement data and the modeling are considered using the Bayesian method. The detection of the three damage cases with the proposed elimination of the temperature effect on frequencies is shown in Figs. 14–16. In particular, Fig. 14 shows that the slightest damage (d_e = 5 mm) can be identified successfully with the D-S fusion. The damage detection results of damage case d_e = 10 mm are shown in Fig. 15. The true damaged element can be detected correctly, and the probability of a false identification is low. The results are more accurate than those in Fig. 12, in which the temperature effect is not eliminated. These observations demonstrate that the elimination of the temperature effect on frequencies can improve the damage detection results, especially for slight damages. Fig. 16 shows the damage detection results of damage case d_e = 15 mm, in which the damage is correctly located, and false identification has lower probability than when the temperature effect is neglected.

This investigation demonstrates that the individual damage detection is still dramatically affected by uncertainty, even if the temperature effect has been removed. For example, Fig. 15(a) shows that the individual results of “Test 1” indicate that the damage is on element 2; however, the individual results of “Test 2” show that elements 2 and 11 are damaged. The damage detection results are inconsistent among the different tests. Similar phenomena are also observed in Figs. 14(a) and 16(a). To this end, the data fusion technique is required to combine these individual results to obtain a consistent result.

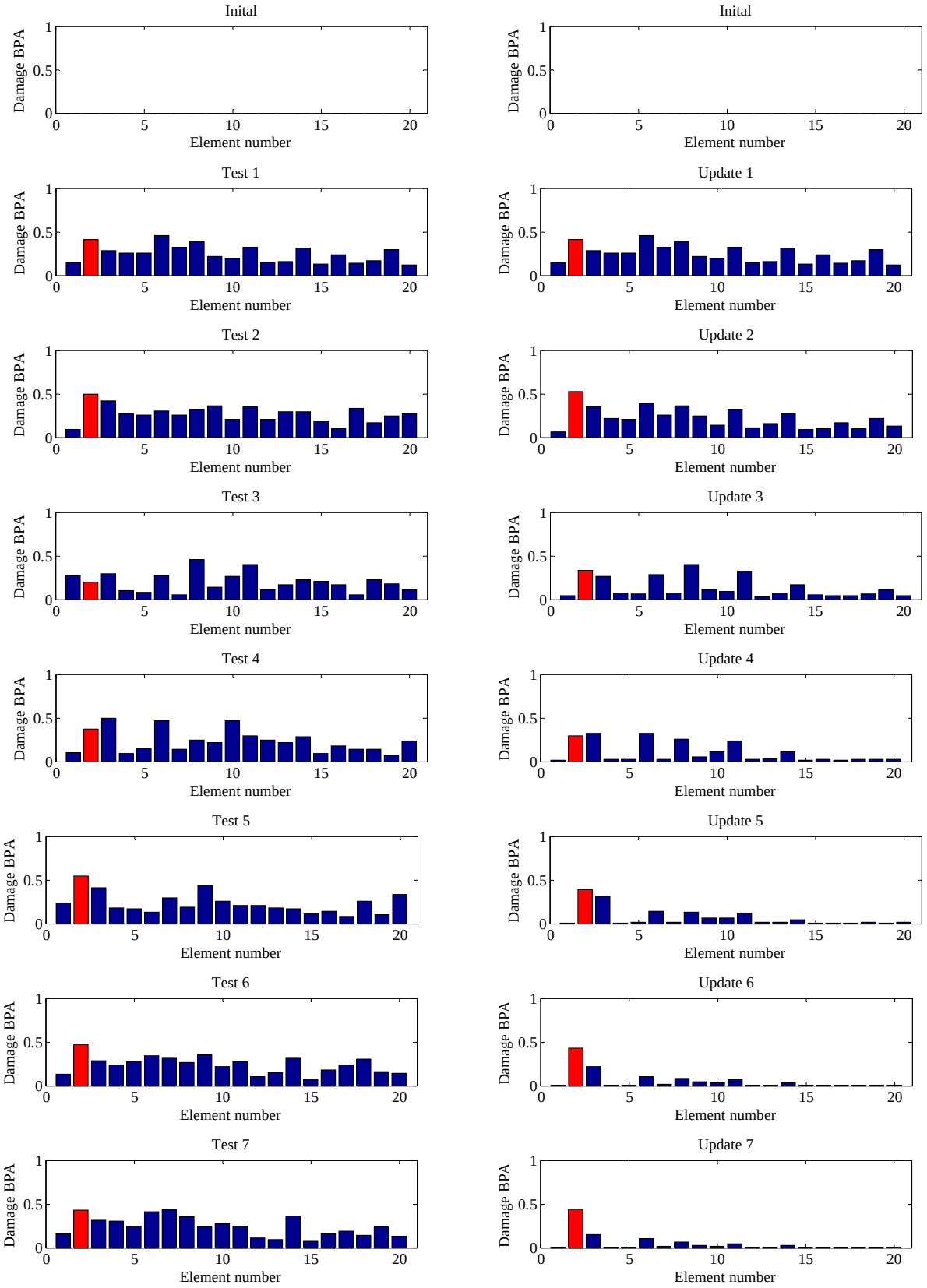

(a) Each test result (b) D-S fusion results

Fig. 14. Damage detection results of damage case d_e = 5 mm after eliminating the temperature effect

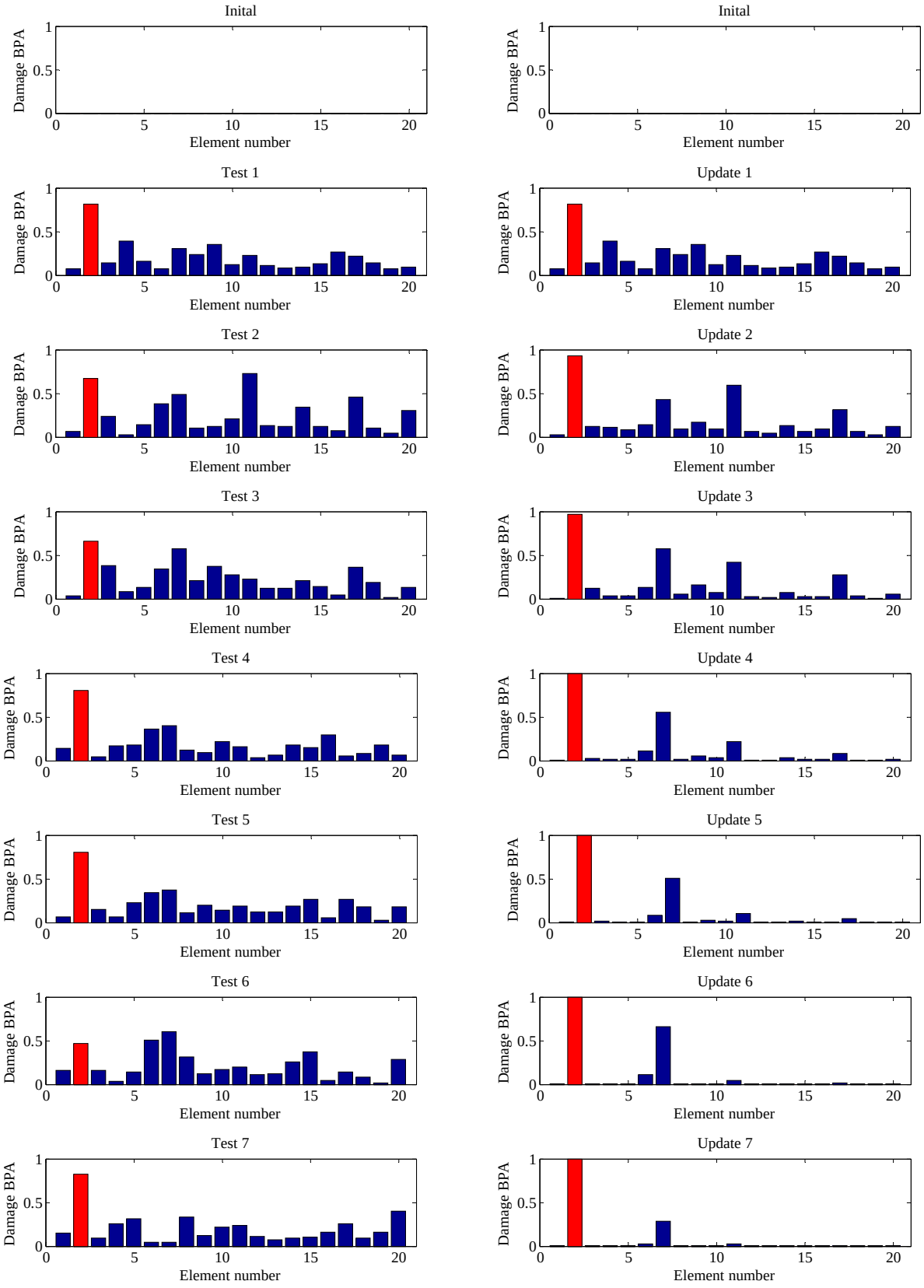

(a) Each test result (b) D-S fusion results

Fig. 15. Damage detection results of damage case d_e = 10 mm after eliminating the temperature effect

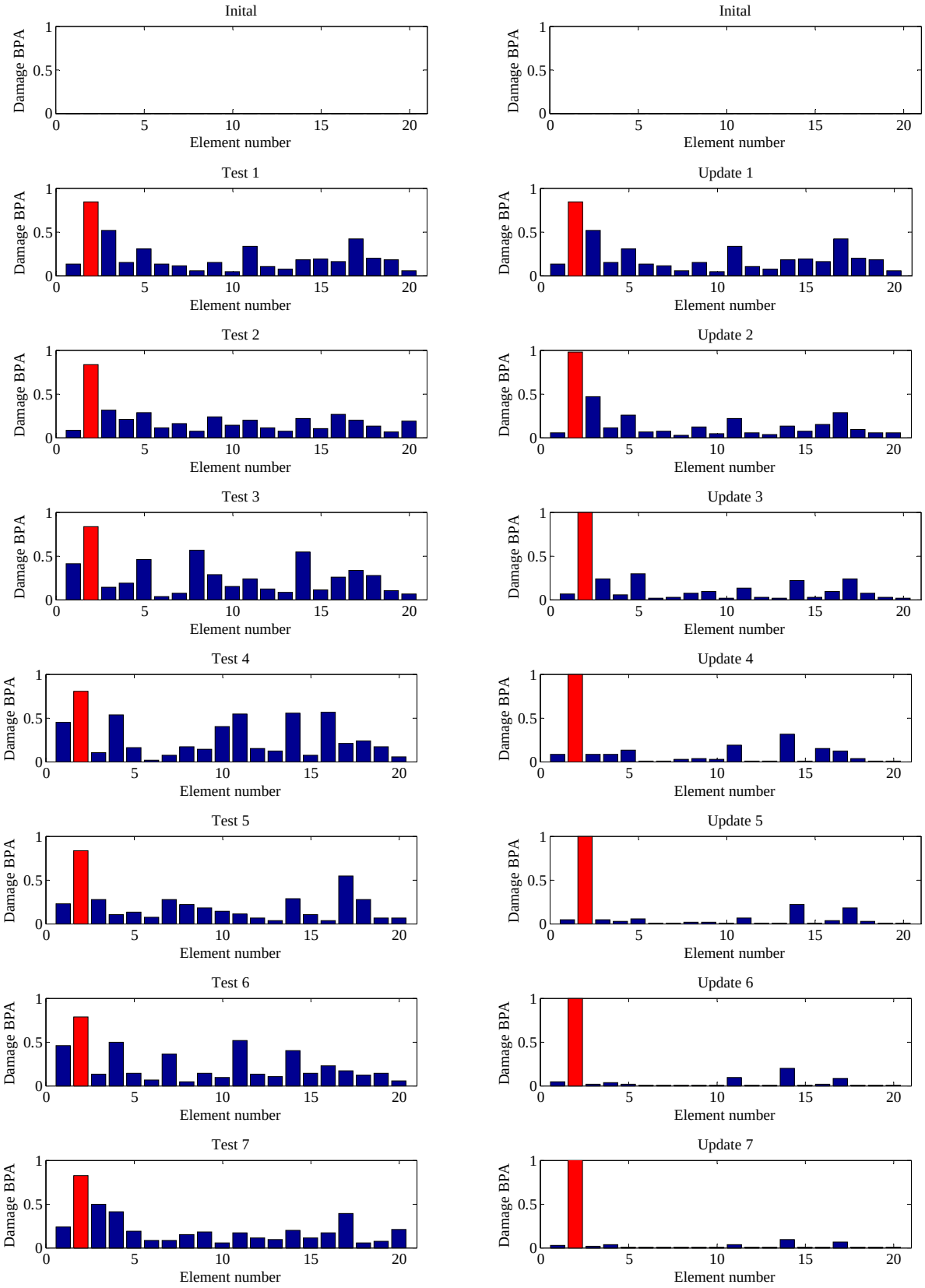

(a) Each test result (b) D-S fusion results

Fig. 16. Damage detection results of damage case d_e = 15 mm after eliminating the temperature effect

5 Conclusions

A data fusion-based damage detection method, with consideration on the temperature effect, is proposed. A series of experiments is carried out on a two-storey steel frame under different temperature conditions to verify the effectiveness of the proposed method in damage detection.

The temperature has a significant effect on the vibration frequencies in a linear manner approximately, whereas it has little effect on mode shapes. Based on the linear relation between the frequencies and temperature, the frequencies measured under different temperature conditions can be transformed into those at the reference temperature. Consequently, the frequencies of the undamaged and damaged structures can be regarded as the measurements under the same temperature.

The temperature effect on the frequencies masks the effect of the damage, especially when there is slight damage on the element. The damage detection results, with the elimination of the temperature effect, are improved, especially for slight damage, compared with those in which temperature variation is not considered.

Uncertainties in the measurement noise and finite element modeling may result in the true damages not being detected correctly, even when the temperature effect on the vibration measurements has been removed. Combination of the BPAs from different sets of data using the D-S approach can reduce the false identification induced by these uncertainties. Thus, the damages can be detected more accurately than those using the measured data separately. The measurement noise, modeling error, and environmental variation are considered in an integrated manner. The experimental results demonstrate that the method improves the accuracy and reliability of vibration-based damage detection methods.

Acknowledgments

The work described in this paper was supported by the Hong Kong Polytechnic University Research Grant (Project No. A-PJ14) and grants from the National Science Funding China (Grant No. 51008095).

References

[1] H. Sohn, C.R. Farrar, F.M. Hemez, D.D. Shunk, D.W. Stinemates and B.R. Nadler, A review of structural health monitoring literature: 1996-2001, Los Alamos National Laboratory Report, LA-13976-MS (2003).

[2] Y. Xia, H. Hao, J.M.W. Brownjohn and P.Q. Xia, Damage identification of structures with uncertain frequency and mode shape data. *Earthq. Eng. Struct. D.* **31**(5) (2002) 1053-1066.

[3] X.Q. Zhu and H Hao, Damage detection of RC Slabs Using Nonlinear Vibration Features, *Int. J. Struct. Stabil. Dyna.* **9**(4) (2009) 687-709.

[4] J.M.W. Brownjohn, Structural health monitoring of civil infrastructure, *Phil. Trans. R. Soc. A.*, **365** (1851) (2007) 589-622.

[5] Z. Wang, F.T.K. Au and Y.S. Cheng, Statistical damage detection based on frequencies of sensitivity-enhanced structures, *Int. J. Struct. Stabil. Dyna.* **8**(2) (2008), 231-255.

[6] A. Dromigny and Y.M. Zhu, Improving the dynamic range of real-time X-ray imaging systems via Bayesian fusion, *J. Nondestr. Eval.* **16** (1997) 147-160.

[7] P. Lucas, Bayesian model-based diagnosis, *Int. J. Approx. Reason.* **27** (2001) 99-119.

[8] J.L. Beck and L.S. Katafygiotis, Updating models and their uncertainties. I: Bayesian statistical framework, *J. Eng. Mech.*, *ASCE* **124**(4) (1998) 455–461.

[9] L.S. Katafygiotis and J.L. Beck. Updating models and their uncertainties. Ⅱ: Model identifiability, *J. Eng. Mech.*, *ASCE* **124**(4) (1998) 463-467.

[10] M.W. Vanik, J.L. Beck and S.K. Au, Bayesian probabilistic approach to structural health

monitoring, *J. Eng. Mech.*, *ASCE* **126**(7) (2000) 738-745.

[11] O. Basir and X.H. Yuan, Engine fault diagnosis based on multi-sensor information fusion using Dempster-Shafer evidence theory, *Inform. Fusion* **8**(4) (2007) 379-386.

[12] B.S. Yang and K.J. Kim, Application of Dempster-Shafer theory in fault diagnosis of induction motors using vibration and current signals, *Mech. Syst. Signal Process*. **20** (2006) 403-420.

[13] K. Worden, G. Manson and T. Denoeux, An evidence-based approach to damage location on an aircraft structure, *Mech. Syst. Signal Process*. **23**(6) (2008) 1792-1804.

[14] M. Sanayei, S.W. Doebling, C.R. Farrar, S.W. Fascetti and B. Arya, Challenges in parameter estimation for condition assessment of structures. World Structures Congress, San Francisco, CA, USA (1998).

[15] T.J. Wipf, Use of tilt sensing equipment for monitoring long-term bridge movement, *Canadian J. Civil Eng.* **18** (1991) 1033-1046.

[16] H. Sohn, M. Dzwonczyk, E.G. Straser, A.S. Kiremidjian, K.H. Law and T. Meng, An experimental study of temperature effect on modal parameters of the Alamosa Canyon Bridge, *Earthq. Eng. Struct. D.* **28** (1999) 879-897.

[17] B. Peeters, G.D. Roeck, One-year monitoring of the Z24-Bridge: environmental effects versus damage events, *Earthq. Eng. Struct. D.* **30** (2001) 149-171.

[18] J.M. Ko, K.K. Chak, J.Y. Wang, Y.Q. Ni and T.H.T. Chan, Formulation of an uncertainty model relating modal parameters and environmental factors by using long-term monitoring data, *Proceedings Smart Structures and Materials: Smart Systems and Nondestructive Evaluation for Civil Infrastructures*, vol. 5057, San Diego CA, USA, pp. 298-307 (2003).

[19] Y. Xia, H. Hao, G. Zanardo and A.J. Deeks, Long term vibration monitoring of a RC slab: temperature and humidity effect, *Eng. Struct.* **28** (2006) 441-452.

[20] Y. Xia, Y.L. Xu, Z.L. Wei, H.P. Zhu and X.Q. Zhou, Variation of structural vibration characteristics versus non-uniform temperature distribution, *Eng. Struct.*, **33**(1) (2011), 146-153.

[21] H.R. Kess and D.E. Adams. Investigation of operational and environmental variability effects on damage detection algorithms in a woven composite plate, *Mech. Syst. Signal Process*. **21** (2007) 2394-2405.

[22] E. Balmes, M. Basseville, L. Mevel and H. Nasser, Handling the temperature effect in vibration monitoring of civil structures: A combined subspace-based and nuisance rejection approach, *Control Eng. Pract.* **7** (2008) 80-87.

[23] Z.D. Xu and Z.S. Wu. Simulation of the effect of temperature variation on damage detection in a long-span cable-stayed bridge, *Struct. Health Monit.* **6** (2007) 177-189.

[24] A.M. Yan, G. Kerschen, P.De. Boe and J.- C. Golinval, Structural damage diagnosis under varying environmental conditions-part 1: A linear analysis, *Mech. Syst. Signal Process*. **19** (2005) 847-864.

[25] Y. Bao, H. Li, Y. An and J. Ou, Dempster-Shafer evidence theory approach to structural damage detection, *Struct. Health Monit.*, DOI: 10.1177/1475921710395813 (2011).

[26] D.L. Hall, *Mathematical Techniques in Multi-Sensor Data Fusion* (Boston: Artech House, 1992).

[27] L.A. Klein, *Sensor and Data Fusion: A Tool for Information Assessment and Decision Making* (SPIE, July 2004).

[28] G. Shafer, *A Mathematical Theory of Evidence* (Princeton University Press, New Jersey, 1976).

[29] R. Yager, On the Dempster-Shafer framework and new combination rules. *Inform. Sciences* **41**(1987) 93-137.

[30] T. Inagaki, Interdependence between safety-control policy and multiple-seonsor schemes via Dempster-Shafer theory, *IEEE Trans. Reliab.* **40**(2) (1991) 182-188.

[31] K. Sentz and S. Ferson, Combination of evidences in Dempster-Shafer theory, Technique Report, Report No. SAND2002-0835, Sandia National Laboratories (2002).

[32] M.W. Vanik, J.L. Beck and S.K. Au. Bayesian probabilistic approach to structural health monitoring, *J. Eng. Mech., ASCE* **126**(7) (2000) 738-745.

[33] C. Papadimitriou, J.L. Beck and L.S. Katafygiotis, Asymptotic expansions for reliability and moments of uncertain systems, *J. Eng. Mech., ASCE* **123**(12) (1997) 1219-1229.

[34] D.J. Ewins, *Modal Testing-Theory, Practice and Application* (Research Studies Press Ltd, UK, 2000).